Multiple unconventional charge density wave transitions in LaPt2Si2 superconductor clarified with high-energy X-ray diffraction

communications materials

ARTICLE

https://doi.org/10.1038/s43246-023-00406-y OPEN

Multiple unconventional charge density wave transitions in $LaPt_2Si_2$ superconductor clarified with high-energy X-ray diffraction

Elisabetta Nocerino[1✉], Irene Sanlorenzo[2,3], Konstantinos Papadopoulos[4], Marisa Medarde[5], Jike Lyu[5], Yannick Maximilian Klein[5], Arianna Minelli[6], Zakir Hossain[7], Arumugam Thamizhavel[8], Kim Lefmann[2], Oleh Ivashko[9], Martin von Zimmermann[9], Yasmine Sassa[4] & Martin Månsson[1✉]

The quasi-2D platinum-based rare earth intermetallic $LaPt_2Si_2$ has attracted attention as it exhibits strong interplay between charge density wave order and superconductivity. However, most of the results reported on this material come from theoretical calculations, preliminary bulk investigations and powder samples, which makes it difficult to uniquely determine the temperature evolution of its crystal structure and, consequently, of its charge density wave transition. Therefore, the published literature around $LaPt_2Si_2$ is often controversial. Here, by means of high-resolution synchrotron X-ray diffraction data, we clarify some of the poorly or partially understood aspects of the physics of $LaPt_2Si_2$. In particular, we resolve the complex evolution of its crystal structure and superstructures, identifying the temperature dependence of multiple density wave transitions in good quality $LaPt_2Si_2$ single crystals. According to our findings, on cooling from room temperature $LaPt_2Si_2$ undergoes a series of subtle structural transitions which can be summarised as follows: second order commensurate tetragonal (*P4/nmm*)-to-incommensurate structure followed by a first order incommensurate-to-commensurate orthorhombic (*Pmmn*) transition and then a first order commensurate orthorhombic (*Pmmn*)-to-commensurate tetragonal (*P4/nmm*). The structural transitions are accompanied by both incommensurate and commensurate superstructural distortions of the lattice. The observed behavior is compatible with discommensuration of the CDW in this material.

[1] KTH Royal Institute of Technology, Department of Applied Physics, Alba Nova University Center, Stockholm SE-114 21, Sweden. [2] Nanoscience Center, Niels Bohr Institute, University of Copenhagen, Universitetsparken 5, 2100 Copenhagen, Denmark. [3] Department of Applied Science and Technology, Politecnico di Torino, corso Duca degli abruzzi 24, 10129 Torino, Italy. [4] Department of Physics, Chalmers University of Technology, SE-412 96 Göteborg, Sweden. [5] Laboratory for Multiscale Materials Experiments, Paul Scherrer Institute, CH-5232 Villigen PSI, Switzerland. [6] Inorganic Chemistry Laboratory, University of Oxford, Oxford OX1 3QR, UK. [7] Department of Physics, Indian Institute of Technology, Kanpur, Uttar Pradesh 208016, India. [8] DCMPMS, Tata Institute of Fundamental Research, Mumbai, Maharashtra 400005, India. [9] Deutsches Elektronen-Synchrotron DESY, Notkestr. 85, 22607 Hamburg, Germany. ✉email: nocerino@kth.se; condmat@kth.se

A grand challenge in condensed matter physics is understanding the mechanisms underlying high-temperature superconductivity (SC). Materials with competing electron spectrum instabilities, such as Cooper pairing and charge/spin-density waves (CDW/SDW), represent the ideal playground for this kind of investigations since the electron–phonon coupling established in such systems is believed to be a key factor in inducing SC[1–4]. The quasi-2D Pt-based rare earth intermetallic material $LaPt_2Si_2$ belongs to this family of compounds as it exhibits strong interplay between CDW and SC. $LaPt_2Si_2$ crystallizes in a $CaBe_2Ge_2$-type tetragonal structure (space group $P4/nmm$), where two non-equivalent layers (Si1-Pt2-Si1) and (Pt1-Si2-Pt1) are arranged in alternating stacking separated by lanthanum atoms. In single-phased powder samples, indications of a first-order structural transition were observed from high-temperature tetragonal to low-temperature orthorhombic symmetry, accompanied by a CDW transition at around $T_{CDW} = 112$ K[5,6]. Here superlattice reflections corresponding to (n/3, 0, 0), with $n = 1$ and 2 were observed, followed by a SC transition at $T_c = 1.22$ K. It was suggested by Nagano and coworkers that the CDW modulation of the crystal lattice would induce a tripling of the initial unit cell and that it would propagate in the Pt2 layer, while superconductivity would be established separately in the Pt1 layer[6]. The Fermi surface of $LaPt_2Si_2$ was found to have a two-dimensional nature[7] and theoretical calculations of the phonon dispersion curves predicted phonon-softening instabilities[8], leading to structural instabilities, that would be compatible with the putative (1/3, 0, 0) Q-vector of the CDW observed by Nagano and coworkers[6]. However, contrary to the aforementioned conjecture of Nagano[6], it was also shown that CDW and SC should coexist in the Pt1 layer[7] and the softened phonon modes would mainly arise from Pt1. This finding suggested that the CDW transition occurs in the Pt1 layers, with large electron–phonon interaction[8], which was later confirmed by Pt-NMR measurements[9]. Beyond the results on polycrystalline samples[10], single-crystal diffraction studies with in-house characterization methods were also reported[11]. According to these studies, the CDW transition occurs at 85 K (slightly lower in comparison to the 112 K for polycrystalline samples) in correspondence to the maximum intensity of superlattice satellites which were found to have propagation vector $\mathbf{q}1 = (0.36\ 0\ 0)$. This value is slightly different from the previously reported (1/3 0 0), indicating that the CDW modulation is actually incommensurate and suggesting that the properties of this material as a single crystal might be different from the ones as a polycrystal. Also, there was no clear indication of a structural transition towards orthorhombic crystal symmetry in single-crystalline $LaPt_2Si_2$[11], so its low-temperature crystal structure could not be resolved. In addition, the CDW-induced modulation of the lattice has more recently been found to develop a periodicity also along the c axis with a different propagation vector and a different temperature dependence with respect to the previously identified one, which solely propagates in the ab-plane[12]. This new periodicity, resulting in an additional set of satellites in the diffraction pattern with a propagation vector $\mathbf{q}2$ different from the one previously identified $\mathbf{q}1$, seemed to indicate that multiple CDWs develop in this material. Here, the first one was assigned to a high-temperature transition occurring within a suggested temperature range $160\ \mathrm{K} < T < 175\ \mathrm{K}$, and the second one was assigned to the low-temperature transition at $T = 85$ K, already identified in the previous report in reference[11]. The first high-temperature transition has been so far disregarded in the literature, because there was no indication that $LaPt_2Si_2$ should have two CDW transitions. Moreover, the low-temperature transition displayed more obvious manifestations with respect to the high-temperature one in basic characterization methods (i.e., sharp anomalies in specific heat, electrical resistivity and such). The authors of reference[12] argue that the results of bulk characterization methods previously reported for $LaPt_2Si_2$ should be reinterpreted under the light of this additional transition, and that high-resolution X-ray diffraction measurements would be needed to resolve the temperature evolution of the crystal structure and superstructure in this material. Finally, the superconductivity in $LaPt_2Si_2$, initially identified as non-conventional (the Fermi surface exhibits two gaps of different magnitude according to μ^+SR measurements[13]), was recently found to have a SC gap and London penetration depth well described by a standard BCS model[14].

As can be inferred from the above summary, the published literature about the structural and electronic properties of $LaPt_2Si_2$ can be often found to be inconsistent and sometimes contradictory. At the time of performing the experimental work and data analysis presented below, there were no reports showing the phonon dispersion curves in $LaPt_2Si_2$ which could confirm the theoretical predictions and provide direct evidence of the CDW transition as well as its temperature evolution. Moreover, the low-temperature crystal structure, in the CDW phase, was not solved for powder nor for single-crystalline $LaPt_2Si_2$.

Our work clarifies the complex evolution of the crystal structure in this material as well as the true temperature dependence and nature of its CDW state. In particular, in this paper we investigate the details of the temperature-dependent structural and superstructural evolution of $LaPt_2Si_2$ single crystal with high-resolution synchrotron XRD. On cooling from room temperature, we recorded a series of subtle structural transitions occurring in this material for which the crystal goes from a commensurate tetragonal crystal structure (space group $P4/nmm$) to an incommensurate structure, through a smooth gradual transition having its onset at $T = T1 = 230$ K. Further, upon reaching a temperature $T = T2 = 110$ K, $LaPt_2Si_2$ undergoes an abrupt transition from the incommensurate structure to a commensurate orthorhombic structure (space group $Pmmn$). Finally, another abrupt transition occurs at $T = T3 = 60$ K, which brings the system from the commensurate orthorhombic structure ($Pmmn$) to a commensurate tetragonal structure (space group $P4/nmm$). Such restructuring of the main crystal symmetry is accompanied by both incommensurate and commensurate modulations of the unit cell, resulting in the formation of three sets of superstructural Bragg satellites, i.e., the previously identified $\mathbf{q}1$ and $\mathbf{q}2$, as well as a third set of satellites $\mathbf{q}3$, observed in this work for the first time. Following the temperature evolution of the $\mathbf{q}1$ and $\mathbf{q}2$ satellites, they were found to display temperature-dependent fluctuations in their intensities. Such behavior is suggestive of a non conventional character of the CDW state established in $LaPt_2Si_2$. We also present the results of bulk characterization methods where we highlight the subtle anomalies in correspondence of the so far hidden in plain sight high-temperature CDW transition.

Results

Bulk measurements. Figure 1a, b displays resistivity data, collected both on heating and cooling in the temperature range from 1.5 to 300 K, on a $LaPt_2Si_2$ single-crystalline sample with the electric current running along the c axis. Figure 1c, d displays the magnetic susceptibility curve measured under magnetic fields equal to 0.5 T, 2 T, 5 T, and 7 T, applied along a axis and c axis.

The sharp drop in the resistivity curve between 2 K and the lowest measured temperature 1.5 K, is most likely due to the onset of the superconducting transition, reportedly occurring at $T_c = 1.22$ K. The curve between 2 and 100 K is well fitted to a power law below 50 K and to a straight line above, as usually occurs in normal metals. The value of the exponent resulting

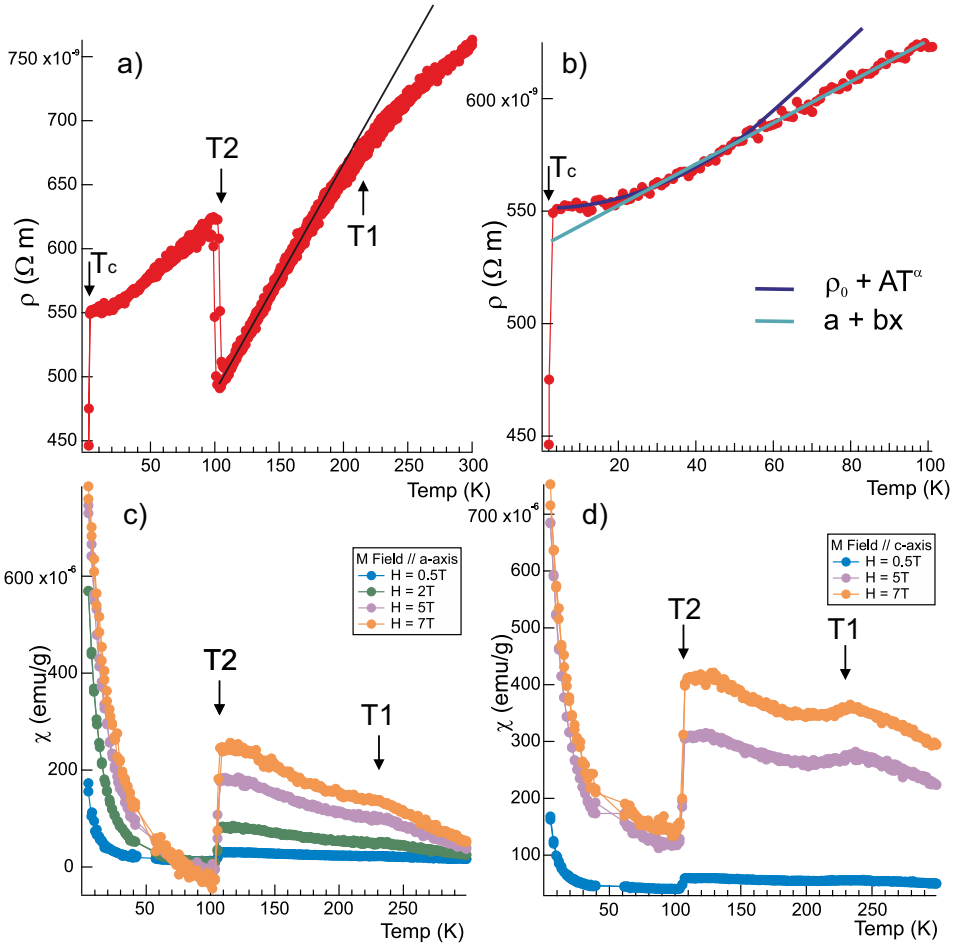

Fig. 1 Bulk characterization results for $LaPt_2Si_2$. a Resistivity curve as a function of temperature for $LaPt_2Si_2$ single crystal with the electric current applied along the *c* axis, the solid line is a guide to the eye to highlight the change of slope in the resistivity curve. **b** Detail of the resistivity curve in the temperature range from 2 to 100 K. The solid lines are fits to the power law and linear functions, respectively. **c** Susceptibility curve for $LaPt_2Si_2$ with the magnetic field flux lines oriented along the *a* axis and **d** *c* axis with different values of the field magnitude. The confidence intervals of the reported values are represented in the plots by the error bars on the experimental points.

from the power law fitting is $\alpha = 2.1 \pm 0.1$, which is the signature of normal Fermi liquid behavior and suggests that no strong electron-electron interactions are in place in this system[15]. This could be indication of the fact that the superconducting state established in $LaPt_2Si_2$ is of conventional nature, however deeper analysis in needed to unambiguously support such a statement. A sharp anomaly in the resistivity curve is observed in the proximity of $T2 = 110$ K, corresponding to the previously identified CDW transition and, as will be clarified in the next section, concomitant with a first-order transition of the crystal structure as well as with the appearance of the **q**2 satellites. In simple Peierls systems this transition is suggestive of a gap opening at the Fermi surface and usually occurs between a metallic and an insulating phase[16]. However, the presence of a metallic behavior below the transition in $LaPt_2Si_2$ indicates that the gap opening in this system is partial and does not take place over the entire Fermi surface. Interestingly, the resistivity curve above $T2$ deviates from linearity with a rate decrease (i.e., bending downwards), displaying a phenomenology similar to the prototypical 2-dimensional CDW material $NbSe_2$[17]. In $LaPt_2Si_2$, the deviation from linearity occurs at the temperature $T1 = 230$ K which, as will be clarified in the next section, corresponds to the onset of a continuous commensurate-to-incommensurate structural transition, to the appearance of the **q**1 satellites and, therefore, to the actual high-temperature CDW transition in $LaPt_2Si_2$. A possible interpretation for the negative curvature of the resistivity at $T1$, is that it is caused by local fluctuations of the CDW causing the opening of gaps on the Fermi surface which are too small to conspicuously affect the transport properties of $LaPt_2Si_2$ in the high-temperature range[17].

A pronounced first-order anomaly in the temperature dependence of the magnetic susceptibility (Fig. 1c, d) is observed in proximity of $T2$, indicating a reduction in the electronic density of states due to partial opening of a gap at the Fermi surface. Differences between data with magnetic fields applied along *a* and *c* axes imply anisotropy of the gap. A small anomaly in the susceptibility is observed in proximity of $T1$ which, consistently with the negative curvature of the resistivity data, likely indicates the aforementioned small gap opening in correspondence to the high-temperature CDW transition. The published literature has not discussed this high temperature transition in the susceptibility data, as well as the negative curvature of the resistivity above $T2$. Since $LaPt_2Si_2$ was not expected to host multiple CDW transitions, previous reports had always attributed the low-temperature first-order transition at $T2$ to the only CDW transition expected in this system. With the results reported in this paper, it is now possible to re-interpret these bulk measurements by placing the high-temperature CDW-induced gap opening in correspondence to the small anomaly in the susceptibility/resistivity at $T1$, and by associating the sharp

transition at $T2$ to a change in the electronic states of $LaPt_2Si_2$, induced by the first-order structural transition from distorted tetragonal to orthorhombic crystal symmetry, in correspondence to the low-temperature CDW transition.

Synchrotron XRD measurements. The diffraction measurements reported here were carried out in two different beam-attenuation settings: atten2 and atten0 (for more details concerning the experimental set-up, refer to "Methods"). The atten2 dataset is well suited for structural analysis, while the higher intensity of the atten0 dataset allows the detection of diffuse scattering and weak superstructural Bragg reflections. Due to the saturation of the structural Bragg peaks in the atten0 setting, the atten2 data were used for refinement of the underlying crystal structure of $LaPt_2Si_2$ and accurate determination of the temperature dependence of the satellites. The atten0 data are shown for clarity of display of the weak satellites and diffuse scattering. The scattering data have been acquired through angular scans of the $LaPt_2Si_2$ single crystal that could cover the full 3-dimensional angular range. The white lines, that are visible in all the diffraction data shown in this work, are due to the gaps between the individual tiles of the Pilatus 2M detector as they appear in the reconstructed reciprocal lattice planes.

Temperature dependence of 2-dimensional diffraction data. Figure 2a–c shows the reciprocal space planes [h k 0] (in atten2 setting), [h k 0.5] (in atten0 setting) and [h k 0.25] (in atten2 setting), for few selected temperature points $T =$ 300 K, 205 K, 92 K, 24 K. Such planes were obtained by reconstructing the diffraction data in a single layer defined by the L1 = (1 0 0) and L2 = (0 1 0) vectors with the origin in (0 0 0), (0 0 0.5) and (0 0 0.25) reciprocal lattice units respectively. Well-structured diffuse scattering, indicating the presence of interactions with short-range correlation lengths in the *ab*-plane, induced by charge ordering, is already present at $T = 300$ K. Since the diffuse scattering does not converge on Bragg peaks at integer hk coordinates, but it rather lies around them at non-integer positions, the possibility of thermal diffuse scattering is excluded. This implies that the charge ordering that results in the multi-q modulation of the lattice is already in place in this temperature range. Therefore, the onset of the charge ordering in $LaPt_2Si_2$ is well above room temperature. The atten0 setting was chosen in the representation of the [h k 0.5] plane to highlight the presence of the diffuse scattering, since no structural Bragg peaks are allowed in this region of the reciprocal space and their oversaturation would not cause too much disturbance.

As the temperature decreases, we observe the appearance of satellites with 6 different propagation vectors, refined with the data analysis software CrysAlis^{Pro}[18]. Between 235 and 35 K the satellites have average values of the propagation vectors $\mathbf{q}'1 =$ [0.35736 0 0] ≈ [0.36 0 0] and $\mathbf{q}''\mathbf{1} =$ [0 0.35905 0] ≈ [0 0.36 0] in the full temperature range (Fig. 2a). Below 35 K the $\mathbf{q}'1$−$\mathbf{q}''\mathbf{1}$ satellites become weaker (but not enough to completely disappear) and the formation of the satellites $\mathbf{q}'2 =$ [0.18 0.18 0.5] and $\mathbf{q}''\mathbf{2} =$ [0.18 −0.18 0.5] occurs (Fig. 2b). Looking at the reciprocal unit cell projections in the atten0 data at base temperature, a third set of peaks could be identified with propagation vectors $\mathbf{q}'3 =$ [0.3 0.3 0.25] and $\mathbf{q}''\mathbf{3} =$ [−0.3 −0.3 0.25]. This new set of satellites, whose intensity might possibly become stronger at lower temperature, could be noticed only by exploring the reciprocal cell in the zero attenuation data. Once they have been identified, appropriate cuts in the atten2 data allowed the observation of the $\mathbf{q}3$ satellites in this dataset as well, despite the stronger attenuation conditions (Fig. 2c). The plots displaying the [h k 0.25] plane in Fig. 2c, show some diffuse scattering features for temperatures above 24 K. These features are also visible in the [h k 0.5] and [h k 0] sections as diffuse scattering preceding the formation of the $\mathbf{q}2$ satellites, and as Bragg reflections associated to the underlying crystal structure of $LaPt_2Si_2$ respectively. The sharp $\mathbf{q}3$ superlattice spots in the [h k 0.25] plane at low temperature appear with a different in-plane periodicity compared to the diffuse features, and with a fourfold stacking sequence. Thus, the origins of diffuse scattering and $\mathbf{q}3$ superlattice intensities are different. The extension of the diffuse features from the [h k 0.5] and [h k 0] planes along the l direction is either due to limited resolution along this direction or due to disorder between lattice planes stacked along the c axis. It should be mentioned that the possibility of correlated disorder induced by lattice strain as the origin for the diffuse scattering in $LaPt_2Si_2$, such as the one observed in e.g., $BaZrO_3$-doped YBCO thin films[19], can be also ruled out. Indeed, starting from the XRD results reported in this work, we carried out a follow-up inelastic neutron scattering study[20] aimed at the observation of the CDW-driven phonon softening foreseen in this system by theoretical calculations[8]. Here, while inspecting the elastic line for crystal alignment purposes, we tracked the temperature dependence of the $\mathbf{q}1$ satellite (2 −0.36 0). Taking advantage of the fact that neutrons, unlike X-rays, interact with atomic nuclei rather than electronic clouds in the scattering process, we could focus merely on the lattice distortions/structural strain without the contribution of charge ordering. The neutron data show that the intensity of the $\mathbf{q}1$ satellite is completely suppressed at 250 K, and no elastic diffuse neutron scattering could be observed at this q-point. This indicates that the diffuse scattering observed in the XRD measurements above this temperature is solely attributed to charge modulation. This conclusion holds surely for the $\mathbf{q}1$ satellites (from direct measurements), and could be inferred for the $\mathbf{q}2$ satellites given the hierarchical relationship that connects these two propagation vectors (see Eq. (1) and (2) below). Nonetheless, high-temperature single-crystal XRD and neutrons studies might be relevant to follow the trend of the diffuse scattering above room temperature and ultimately confirm its nature. Under the light of our neutron scattering findings[20], showing the phonon-softening instability precursor of the CDW transition being already in place at a temperature as high as 450 K, we would expect the diffuse scattering to be still visible up to this temperature. Figure 3a–g shows an overview of the three sets of satellites through a diagonal cut along the reciprocal space plane [h h l], obtained by reconstructing the diffraction data in a single layer defined by the L1 = (1 1 0) and L2 = (0 0 1) vectors with the origin in (2.18 −2.18 0.5). The resulting cut represents a plane parallel to the l direction oriented along the $k = h - 4.36$ direction in the hk plane. The latter choice for the reciprocal lattice cut allows clear simultaneous observation of satellites belonging to all the 3 sets of propagation vectors. At 300 K the [h h l] plane, displayed in both atten0 (Fig. 3a) and atten2 (Fig. 3e) settings for comparison, shows the presence of the aforementioned well-structured diffuse scattering in correspondence of the reciprocal lattice points where the $\mathbf{q}1$ and $\mathbf{q}2$ satellites are located. Interestingly, the diffuse scattering observed from the [h h l] plane is found in the form of broad discrete scattering spots, unlike the stripe-like shape manifested in the [h k 0] plane (Fig. 2). This would indicate the presence of interactions with long-range correlation lengths along the l direction in reciprocal space, implying that strong coupling is in place between the Pt layers along the c axis already at room temperature. On cooling from 300 K, the $\mathbf{q}1$ satellites become gradually sharper and more intense below 230 K, while the $\mathbf{q}2$ satellites still display weak intensities and broad line shapes (Fig. 3b, c, f). At 24 K (Fig. 3d, g), all the satellites, including the $\mathbf{q}3$ ones, show sharp line profiles along the three directions h, k,

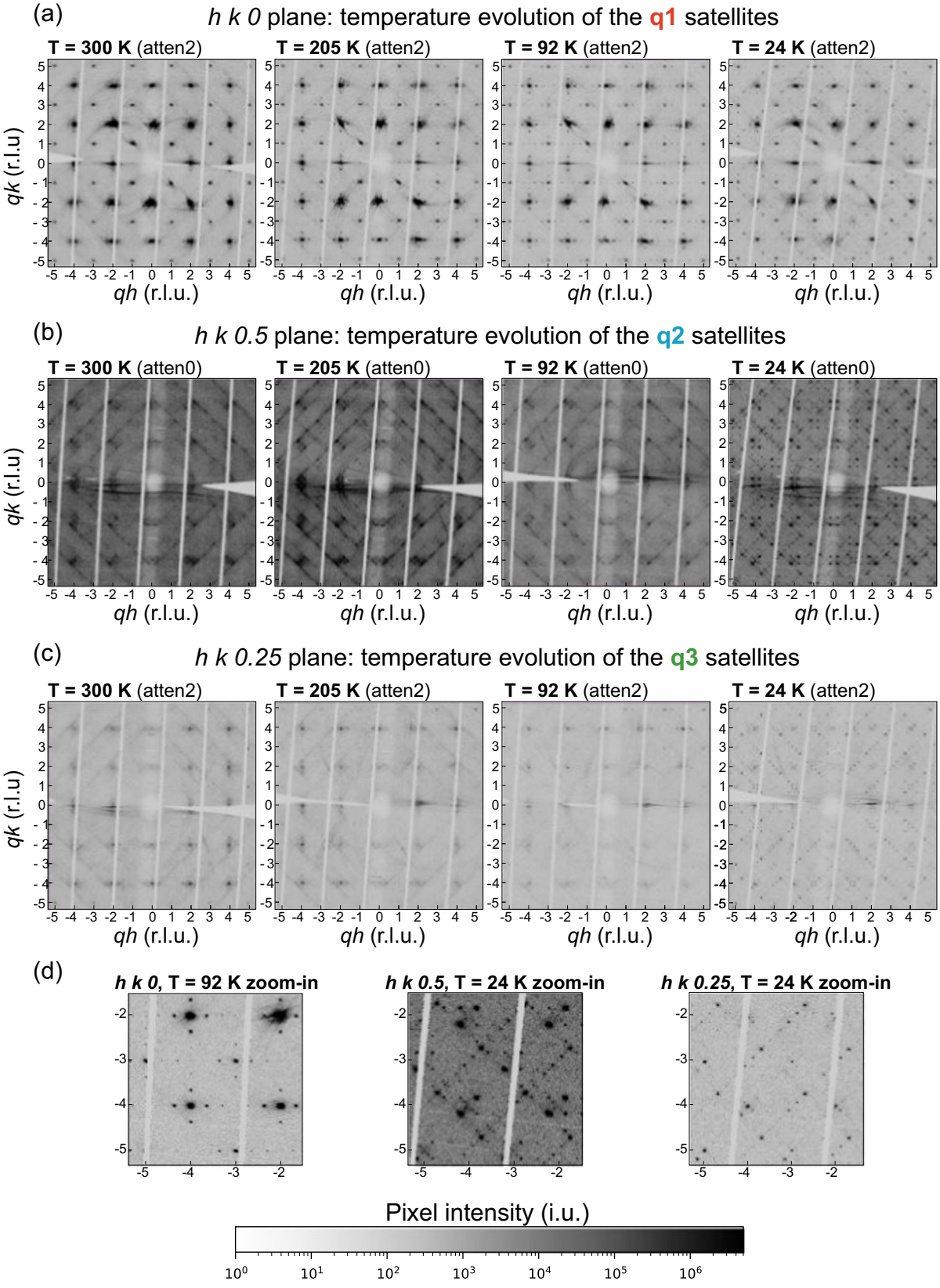

and *l*, which indicates that such lattice modulations have a long 3-dimensional phase coherence length for all the propagation vectors. This would imply strong coupling between and within the Pt layers. It should be noted that, while the appearance of the **q**1 and **q**2 satellites is preceded by diffuse scattering, no detectable diffuse scattering is observed in correspondence of the **q**3 satellites sites prior to their formation. This can be clearly seen by comparing the magnified plots of the [*h h l*] plane at 92 K (Fig. 3f) and 24 K (Fig. 3g), where the **q**1, **q**2, and **q**3 positions are explicitly marked under the plots. Here, we also outlined the [*h k* 0], [*h k* 0.25] and [*h k* 0.5] planes, to show how they cut through the **q**1, **q**3, and **q**2 satellites, respectively.

Fig. 2 Reciprocal lattice planes overview. Comparison between the reciprocal space planes **a** [*h k* 0], **b** [*h k* 0.5], **c** [*h k* 0.25], at 300 K, 205 K, 92 K, and 24 K. **a** The **q**1 modulation is visible, along with the Bragg peaks of the underlying crystal structure. The (**b**) plots are reported in atten0 setting, for clarity of display of the diffuse scattering in the [*h k* 0.5] plane. Here the **q**2 modulation is visible, without the Bragg peaks of the underlying crystal structure. The temperature evolution of the room temperature short-range diffuse scattering, which gradually turns in sharp Bragg satellites, is clearly visible. **c** The **q**3 modulation is visible without the Bragg peaks of the underlying crystal structure. All these cuts are obtained by keeping the *hk*-plane constant, while shifting the *l* axis in non-integer steps. The coordinates on the plots are expressed in reciprocal lattice units (r.l.u.) as (*qh*, *qk*, *ql*). The pixel intensity is reported in intensity units (i.u.), accounting for the number of X-ray counts per pixel. **d** Zoomed-in plots are also shown for selected temperatures to highlight the low-intensity peaks in the three planes.

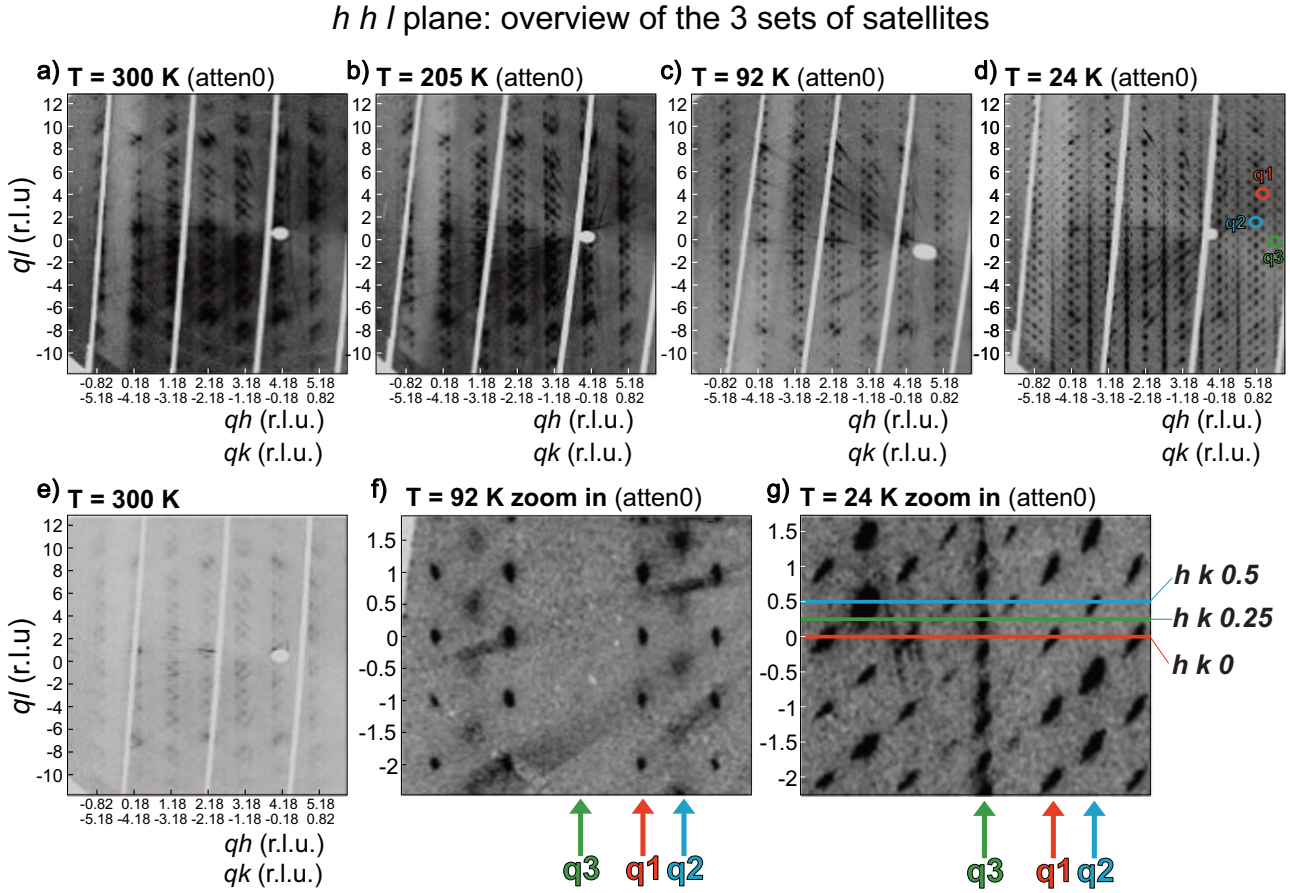

Fig. 3 Reciprocal lattice planes overview. Temperature evolution of the reciprocal space plane [*h h l*] displayed in the atten0 setting at **a** 300 K, showing the room temperature short-range diffuse scattering, **b** 205 K, just below *T*1, **c** 92 K, where the **q**1 satellites display a sharp profile while the **q**2 are still broad, and **d** 24 K, showing the three sets of satellites **q**1 (marked with the red color), **q**2 (marked in blue), and **q**3 (marked in green), all of them having a sharp profile at base temperature. **e** The [*h h l*] plane in room temperature and atten2 setting is also shown here for comparison. **f** Magnified portion of the [*h h l*] plane at 92 K and at (**g**) 24 K. Here the position of the **q**1, **q**2, and **q**3 satellites is explicitly marked along with the cuts in correspondence of the [*h k* 0], [*h k* 0.25], [*h k* 0.5] planes. The reciprocal space cuts displayed in this figure are done along the *l* axis in the *hk* diagonal direction, to allow the simultaneous visualization of the three orders of satellites as they appear in the different temperature regions. The coordinates on the plots are expressed in reciprocal lattice units (r.l.u.) as (*qh*, *qk*, *ql*).

Refinement of the charge density wave propagation vectors. By following the temperature evolution of the intensities and full width at half maximum of the following satellites: [**q**′1 + (0 −4 0)], [**q**′2 + (2 −2 0)] and [**q**′3 + (−2 3 0)] (Fig. 4), four main temperature regimes have been identified. Between 300 K and $T1 = 230$ K a well-structured diffuse scattering corresponding to the **q**1 and **q**2 satellites positions is observed. Between $T1 = 230$ K and $T2 = 110$ K the **q**1 satellites are formed and their intensity increases as the temperature decreases down to 110 K, where an abrupt drop in the satellites intensity is observed. Between $T2 = 110$ K and $T3 = 60$ K the **q**2 satellites are formed, their intensity grows as the temperature decreases and they coexist with the **q**1 satellites down to 60 K, where an abrupt drop in both the **q**1 and **q**2 satellites intensity is observed. Below $T3 = 60$ K the **q**3 satellites are formed, their intensity grows as the temperature decreases and they coexist with the **q**2 satellites, whose intensity shows a similar trend as the **q**3 satellites. The values for *T*1 and *T*2 are chosen as the onset of the falling edge of the FWHM temperature dependence for the **q**1 and **q**2 satellites, i.e., when the peaks become sharp. All these periodic distortions of the lattice seem to have a different nature, which suggests that the origins of their formation are different. The **q**1 satellites are characterized by incommensurate propagation vectors with zero component along the *c* axis, they are connected to the corresponding nesting wave vector **Q** = (1/3 0 0) which, according to previously reported theoretical calculations[8], modulate the Fermi surface in

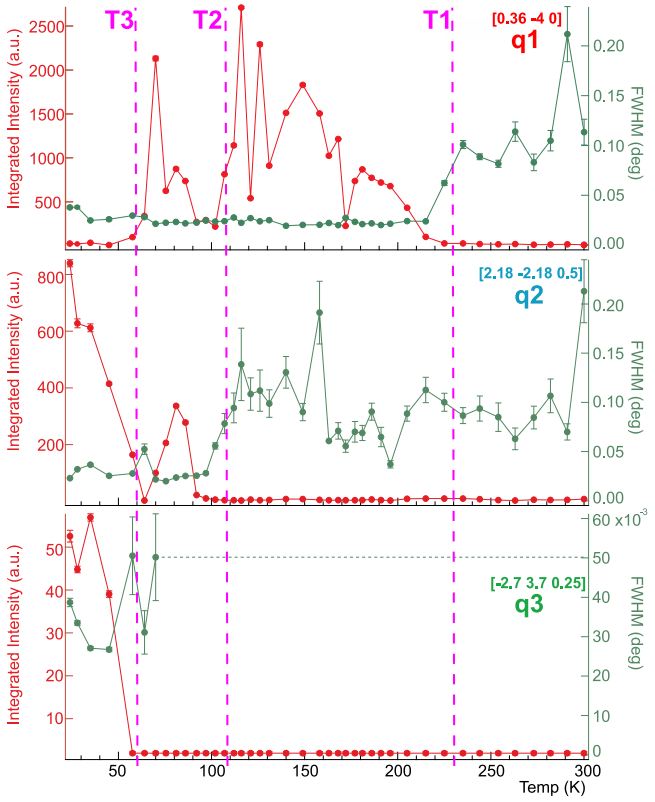

Fig. 4 Temperature dependencies for the 1-dimensional line cuts of selected satellites in $LaPt_2Si_2$. Integrated intensities (left *y* axis) are represented with filled red circles, FWHM (right *y* axis) are represented with filled green circles for three satellites belonging to the three modulations of the lattice **q**1, **q**2, and **q**3, as for the labels on each panel. The transition temperatures *T*1, *T*2, and *T*3 are explicitly marked with magenta dashed lines. The continuous lines between the experimental points are guides to the eye. The confidence intervals of the reported values are represented in the plots by the error bars on the experimental points.

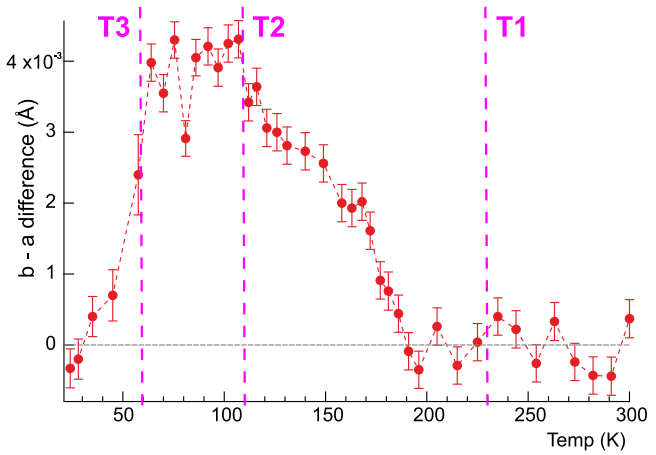

Fig. 5 Difference between the *b* axis and *a* axis in $LaPt_2Si_2$ for the full temperature range. The evolution of the lattice distortions is clearly visible, and the transition temperatures *T*1, *T*2, and *T*3 are explicitly marked with magenta dashed lines. The confidence intervals of the reported values are represented in the plots by the error bars on the experimental points.

$LaPt_2Si_2$ by creating gaps at these positions resulting in the CDW state. The **q**2 satellites are characterized by propagation vectors with incommensurate components in the *ab*-plane and a commensurate component along the *c* axis. The fact that the **q**2 propagation vectors can be expressed as linear combinations of the **q**1 vectors as:

$$\mathbf{q}'2 = \frac{\mathbf{q}'1 + \mathbf{q}''1 + (001)}{2}, \quad (1)$$

$$\mathbf{q}''2 = \frac{\mathbf{q}'1 - \mathbf{q}''1 + (001)}{2}, \quad (2)$$

seems to indicate that the **q**2 satellites are not due to an additional independent CDW *Q*-vector, but are rather related to the **q**1 satellites. In fact, **q**2 appear to be second harmonics of **q**1 since, despite the incommensurate nature of the satellites, the ratio between the components of their respective wave vectors is 2. Here, it is reasonable to assume that **q**2 represents a modification of **q**1, transitioning from a sine-like modulation to a square-like modulation of the lattice. Indeed, by looking at the Bragg satellites characterized by the **q**2 propagation vector, we can see that they exhibit sharp and distinct discontinuities in their intensities both in the [*h k* 0.5] plane (Fig. 2b) and in the [*h h l*] plane (Fig. 3d, g). An abrupt modulation pattern, such as the one here observed, is the signature of a square-like superlattice distortion. The appearance of the **q**2 satellites is also accompanied by the formation of an out-of-plane commensurate modulation of the cell **q**3, probably needed to compensate the structural instability induced by the **q**1 modulation. The **q**3 satellites are characterized by propagation vectors which are linearly independent from **q**1 and **q**2, but their coordinates in the reciprocal space can be expressed in terms of rational fractions of the reciprocal lattice vectors as:

$$\mathbf{q}'3 = \left(\frac{10}{3}(110) + \frac{1}{4}(001)\right), \quad (3)$$

$$\mathbf{q}''3 = \left(-\frac{10}{3}(110) + \frac{1}{4}(001)\right), \quad (4)$$

resulting in a superstructural cell which is quadrupled along the *c* axis. The **q**3 super-cell seems to be just a consequence of the structural instabilities introduced by the incommensurate modulations of the unit cell and, since no detectable diffuse scattering precedes the formation of the **q**3 satellites, it does not seem to be related to any additional CDW nesting vector. However, the very weak intensity of the **q**3 satellites in the atten2 setting, makes the refinement of the **q**3 propagation vectors very difficult. Diffraction measurements at temperatures lower than 24 K, where the intensity of the **q**3 satellites is expected to be enhanced, would be needed for precise determination of their position.

The CDW in this material was previously reported to show indications of a 2-dimensional nature and proposed to develop in the Pt1 layer only[7]. However, our observation of 3-dimensional superlattice distortions and the long-range correlation between the Pt layers seems to point towards a more complex propagation of the CDW in $LaPt_2Si_2$, which probably develops also in the Pt2 layer.

Temperature-dependent structural transitions in $LaPt_2Si_2$. Regarding the evolution of the crystal structure in this system, a change in the lattice parameters occurs as a function of temperature so that the *b* axis becomes gradually longer than the *a* axis, hereby violating the 90-degree rotational invariance about the *c* axis for the known room temperature tetragonal space group *P*4/*nmm*. Figure 5 displays the temperature dependence of the difference $b - a$, which served as a guideline for us to be able to follow the temperature evolution of the crystal structure in $LaPt_2Si_2$. Indeed, the temperature-dependent changes in the unit cell of CDW systems provides valuable information on the formation mechanisms and critical behavior of their CDW phase.

Table 1 Structural parameters in $LaPt_2Si_2$ summary of the space groups, unit cell parameters, atomic coordinates and sites, anisotropic Debye waller factors and reliability *R*-factors of the refinement for $LaPt_2Si_2$ in the three temperature regimes $T > T1$, $T3 < T < T2$ and $T < T3$.

***T* < *T*3**	***T* = 24 K**	**SG: *P4/nmm***		***a* = *b* = 4.2727 (Å),**	***c* = 9.7987 (Å),**	***α* = *β* = *γ* = 90°**		
	x	***y***	***z***	**Occ**	**Site, symm**	**U_{11}**	**U_{22}**	**U_{33}**
Pt1	0.75000	0.75000	0.62009 (4)	1	2c, 4mm	0.00150 (8)	0.00150 (8)	0.00815 (8)
Pt2	0.75000	0.25000	1.00000	1	2a, −4m2	0.0189 (2)	0.0189 (2)	0.0045 (2)
La	−0.25000	0.75000	0.25613 (6)	1	2c, 4mm	0.0022 (1)	0.0022 (1)	0.0069 (2)
Si1	0.75000	0.75000	0.8707 (5)	1	2c, 4mm	0.0113 (11)	0.0113 (11)	0.010 (2)
Si2	0.25000	0.75000	0.50000	1	2b, −4m2	0.0027 (7)	0.0027 (7)	0.0092 (14)
R1 (%)				4.9				
***T*3 < *T* < *T*2**	***T* = 102 K**	**SG: *Pmmn***		***a* = 4.2981 (Å),**	***b* = 4.3021 (Å),**	***c* = 9.876 (Å),**	***α* = *β* = *γ* = 90°**	
-	***x***	***y***	***z***	**Occ**	**Site, symm**	**U_{11}**	**U_{22}**	**U_{33}**
Pt1	0.75000	0.75000	0.62006 (3)	0.5	2a, mm2	0.00544 (7)	0.00266 (10)	0.00675 (11)
Pt2	0.75000	0.25000	1.00010 (3)	0.5	2b, mm2	0.01173 (12)	0.02006 (18)	0.00612 (13)
La	−0.25000	0.75000	0.25608 (4)	0.5	2a, mm2	0.00576 (10)	0.00309 (14)	0.00658 (14)
Si1	0.75000	0.75000	0.8703 (3)	0.5	2a, mm2	0.0102 (9)	0.0117 (11)	0.0084 (9)
Si2	0.25000	0.75000	0.5001 (2)	0.5	2b, mm2	0.0053 (7)	0.0039 (8)	0.0083 (9)
R1 (%)				3.69				
***T* > *T*1**	***T* = 300 K**	**SG: *P4/nmm***		***a* = *b* = 4.2793 (Å),**	***c* = 9.8119 (Å),**	***α* = *β* = *γ* = 90°**		
	x	***y***	***z***	**Occ**	**Site, symm**	**U_{11}**	**U_{22}**	**U_{33}**
Pt1	0.75000	0.75000	0.61995 (3)	1	2c, 4mm	0.00449 (8)	0.00449 (8)	0.0086 (2)
Pt2	0.75000	0.25000	1.00000	1	2a, −4m2	0.01443 (1)	0.01443 (1)	0.00871 (2)
La	−0.25000	0.75000	0.25568 (5)	1	2c, 4mm	0.0051 (1)	0.0051 (1)	0.0083 (2)
Si1	0.75000	0.75000	0.8706 (3)	1	2c, 4mm	0.0095 (7)	0.0095 (7)	0.011 (1)
Si2	0.25000	0.75000	0.50000	1	2b, −4m2	0.0061 (5)	0.0061 (5)	0.009 (1)
R1 (%)				4.3				

Therefore, it is often regarded as an important input for systems exhibiting such instabilities of the electron spectrum[21].

In the context of this work, we assimilate the temperature-dependent difference $b - a$ to an order parameter reflecting the symmetry-breaking phenomena associated with the changes in the $LaPt_2Si_2$ crystal symmetry, caused by the CDW transitions. In the following, the discontinuous jumps at $T2$ and $T3$ in the $b - a$ temperature trend are described as first-order transitions, indicating the sudden structural transitions occurring in $LaPt_2Si_2$ at these temperatures (see dashed lines marking these transitions in Fig. 5). The smooth and continuous increase in the $b - a$ difference observed between $T1$ and $T2$ is instead described as a second-order transition. As clearly seen in Fig. 5, four temperature regimes similar to the ones observed in the temperature evolution of the satellites intensities, can be identified in this case: between 300 K and $T1 = 230$ K the difference $b - a$ is close to zero within the error bars and the crystal structure of $LaPt_2Si_2$ can be reliably refined with the tetragonal space group $P4/nmm$ (no. 129). Between $T1 = 230$ K and $T2 = 110$ K the unit cell is gradually distorted on cooling as the difference $b - a$ grows. In this temperature range, the $\mathbf{q}1$ lattice modulation is incompatible with the tetragonal symmetry and induces a strain resulting in the a and b axes being non-equivalent. Indeed, refinement attempts with the space group $P4/nmm$ could not be stabilized within this temperature range. For this reason, following a group subgroup relationship argument, the centrosymmetric orthorhombic space group $Pmmn$ (no. 59) was initially identified as the most probable solution for a structural transition from a parent space group $P4/nmm$. However, refinement attempts with the latter, as well as with other orthorhombic space groups (namely the noncentrosymmetric $Pmn2$ and $Cmme$) could not provide a stable result either. Indeed, calculations for crystal system recognition including the main unit cell and the $\mathbf{q}1$ modulation vectors for the $T = 140$ K diffraction data, performed with the software Jana[22], provided the triclinic and monoclinic crystal systems as the only possible symmetry choices which would make the main unit cell consistent with the $\mathbf{q}1$ modulation. However, even though in principle the proposed triclinic and monoclinic ($P2_1/m$, $P2/m$, $P2_1$, $P2$) space groups are maximal subgroups of the tetragonal $P4/nmm$, in practice the path of symmetry reductions from the parent structure to such lower symmetry space groups requires several intermediate groups (see the Bärnighausen tree for the $P4/nmm$ space group from the Bilbao Crystallographic Server[23]). This makes the physical realization of such structural transition highly improbable, according to the Symmetry Principle[24]. The most reasonable among the possible monoclinic subgroups is $P2_1/m$, which can be obtained from the aristotype through the path $P4/nmm \rightarrow Pmmn \rightarrow P2_1/m$. However, attempts of refining the $T = 140$ K data with the latter monoclinic space group did not provide any stable result either. Therefore, the structural evolution in the temperature range between $T1 = 230$ K and $T2 = 110$ K will be described as a second-order transition from a commensurate tetragonal phase to an incommensurate distorted phase in which the b axis is elongated with respect to the parent tetragonal structure. The expression "distorted tetragonal" will be used from now on to identify such a phase, in accordance with the wording occasionally used to describe structural phase transitions in martensite alloys[25]. As we keep following the temperature evolution of the $b - a$ difference in Fig. 5, upon reaching the temperature $T2 = 110$ K an abrupt jump in the $b - a$ trend can be observed. Such anomaly is found to correspond to a first-order structural transition occurring between the aforementioned incommensurate distorted tetragonal phase and the centrosymmetric orthorhombic space group $Pmmn$, along with a slight increase in the unit cell volume. The refinement of the crystal structure below T2 could be reliably stabilized with the best R factor achieved for the $T = 102$ K dataset (see Table 1). The R factor becomes progressively worse on cooling from $T = 102$ K to $T = 64$ K. The total amplitude of the displacive distortion between the high and low-temperature crystal structures can be estimated from the structural refinement as $A = 0.0072$ Å. Such a small value for this parameter indicates that the atomic positions in the parent tetragonal structure remain almost unchanged in the orthorhombic cell. However, although the atomic sites of the high-temperature cell are nearly the same as the low-temperature

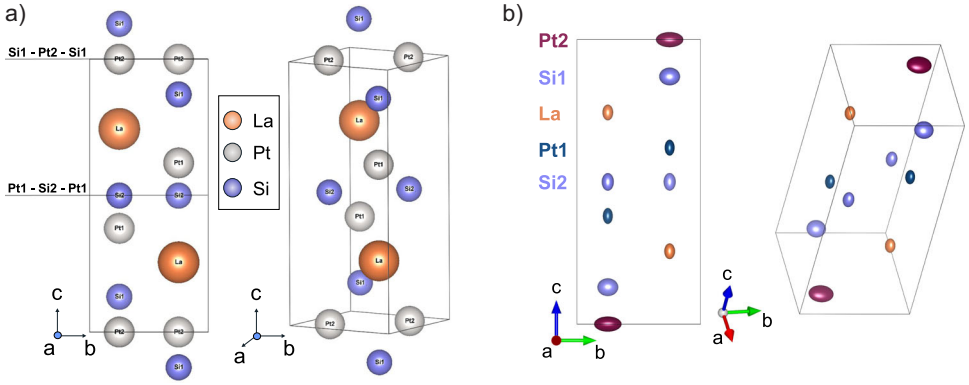

Fig. 6 Refined crystal structure of $LaPt_2Si_2$. a Room temperature unit cell of $LaPt_2Si_2$, lanthanum atoms are represented in orange, platinum atoms in silver, silicon atoms in violet. The alternating Pt–Si planes are explicitly labeled. **b** Unit cell of $LaPt_2Si_2$ with the displacement ellipsoids of the respective atoms. The probability for each atom to be included in the ellipsoids was set to 100%. Beyond the aforementioned colors for the different atomic specimens, here the Pt1 atoms are represented in petrol blue and the Pt2 atoms are represented in burgundy red for clarity of display.

ones, their occupation probabilities undergo a significant change across the transition, as can be seen from the refinement parameters reported in Table 1. This means that the structural change occurring at $T2$ in $LaPt_2Si_2$ is not of displacive nature, but of order-disorder type. It should be noted that for the refinement of the commensurate main phase the satellite Bragg reflections are not taken into account, therefore the low-temperature crystal structures reported here are average crystal structures. The value of the $b-a$ difference remains constant in the temperature range between $T2 = 110$ K and $T3 = 60$ K (Fig. 5). Here, our structural refinement shows that the orthorhombic symmetry is maintained, while the **q**1 and **q**2 satellites coexist (Fig. 4). Below $T3 = 60$ K another first-order structural transition occurs, marked by the abrupt drop in the value of the $b-a$ difference seen in Fig. 5 at $T3$. Here, our refinement of the diffraction pattern at base temperature $T = 24$ K gives again the tetragonal symmetry $P4/nmm$ as a reliable solution for the $LaPt_2Si_2$ crystal structure (see Fig. 6). Therefore, the structural evolution of $LaPt_2Si_2$ can be summarized as follows on cooling from room temperature: tetragonal $P4/nmm \Rightarrow$ distorted tetragonal (2nd order) $\Rightarrow$ orthorhombic $Pmmn$ (1st order) $\Rightarrow$ tetragonal $P4/nmm$ (1st order).

Table 1 reports the results of the refinement within the three temperature regimes $[T < T3]$, $[T3 < T < T2]$ and $[T > T1]$, along with their respective reliability factors R1. The values of the R factor for the three refinements, below 5%, indicate a good agreement between the calculated and observed models. The refinement showed significant improvement with the adoption of an anisotropic displacement parameter **U**. This implies a propensity for the atoms in $LaPt_2Si_2$ to move away from their reference lattice positions along certain privileged directions. In particular, from the values of the diagonal elements of the tensor **U** reported in Table 1 (the refinement provided zero value for the off-diagonal terms), the atoms Pt1 dislocate preferentially along the c axis while the Pt2 within the ab-plane. A graphic representation of the room temperature crystal structure, clearly showing the Pt1 and Pt2 planes, along with the unit cell displaying the anisotropic displacement ellipsoids, extracted from the structural refinement at 102 K, is shown in Fig. 6a, b. This behavior seems to indicate that the Pt2 atoms are responsible for the in-plane coupling of the CDW propagation while the Pt1 atoms are responsible for the out-of-plane coupling along the c axis. This fact is in contrast with the theoretical calculations and the NMR experimental evidence according to which the Pt1 layer is the only responsible for the occurrence of the CDW state in $LaPt_2Si_2$[8,9]. Indeed our results seem to indicate that 2 CDW transitions occur, one at $T = T1 = 230$ K with nesting vectors **q**1, propagating in the Pt2 layer (since **q**1 has l component equal to zero), and a second one at $T = T2 = 110$ K with nesting vectors **q**2, propagating in the Pt1 layer (since **q**2 has nonzero l component). Our recent inelastic neutron scattering study, showing a full collapse of the phonon associated to the (2 0 0) Bragg reflection at $T \sim 230$ K and occurring in a q-region in the surroundings of the related **q**1 satellite (2 0.36 0)[20], also seems to confirm this interpretation.

The reason for the discrepancy between the NMR results and our XRD work might be that the NMR data, which provide proof of the fact that the Pt1-5d bands are the only responsible for the CDW transition in $LaPt_2Si_2$[9], were only acquired in a temperature range from 5 to 200 K, therefore they observed the transition at T2, but not the one at T1. An NMR experiment in a wider temperature range might confirm or disprove this conjecture. It should be noted that a system analogous to $LaPt_2Si_2$ with a $CaBe_2Ge_2$-type structure, $SrPt_2As_2$, shows a double CDW transition occurring in two separate layers[26].

Discussion

The structural instability associated to the formation of CDW eventually results in a structural transition from distorted tetragonal to orthorhombic symmetry in $LaPt_2Si_2$ at $T2 = 110$ K, where ion displacements are needed to stabilize the charge perturbation. Ionic relocation requires strong electron–phonon coupling, which implies that the Fermi surface nesting/gapping cannot be the only driving mechanism involved in this transition, denoting the fact that the CDW established in $LaPt_2Si_2$ cannot be described within the simple Peierls picture. A normal-to-incommensurate structural transition is considered to be strong evidence of CDW formation, and it was indeed observed in the prototypical 2-dimensional layered CDW compound 2H-$TaSe_2$[27] as well as in other systems that exhibit 2-dimensional and 3-dimensional CDWs[25,28]. The phenomenology in these cases foresees an alteration of the normal crystalline periodicity of the material caused by the CDW wave vector which, being determined by the Fermi surface nesting, is not necessarily an integral fraction of the reciprocal lattice vector. In this way an incommensurate structure is established in the crystal, as a result of the distortion of the parent commensurate structure, until the lattice undergoes a second distortion towards a “locked-in” commensurate structure, whose reciprocal lattice vector is an integral multiple of the CDW wave vector. Such structural changes are expected to be second-order (normal-to-incommensurate) and first-order (incommensurate-to-commensurate), respectively, according to the Landau theory of phase transitions, as

demonstrated by McMillan in 1975[29]. In $LaPt_2Si_2$ however, although we observe the occurrence of the second-order normal-to-incommensurate and first-order incommensurate-to-commensurate structural transitions (tetragonal *P*4/*nmm*—distorted tetragonal—orthorhombic *Pmmn*), the lowest energy state with a stable structure does not seem to be achieved in this system within the investigated temperature range. Indeed, an additional first-order structural transition occurs below $T3 = 60$ K. By refining the unit cell parameters together with the incommensurate **q**1 vectors across the temperature range where the **q**1 satellites are clearly visible (70 K < T < 205 K), it is possible to plot the degree of incommensurability δ, defined as $\mathbf{q}'1 = (\frac{1}{3} + \delta\ 0\ 0)$, for the position of the **q**′1 satellites relative to the main lattice as a function of temperature (Fig. 7).

The value of $\delta(T)$ reaches a minimum between 110 and 85 K, which corresponds to the temperature range in which the structural refinement with the orthorhombic unit cell for the main phase shows the best reliability factors (highlighted by the shaded region in Fig. 7), but it is never equal to zero. Indeed the $\delta(T)$ value below 85 K increases again, in correspondence to the increase in intensity of the higher-order satellites **q**2 (see Fig. 4). Although a structural transition to a crystalline commensurate phase can be stabilized in the temperature range 85 K < T < 110 K, it cannot be labeled as a "locked-in" transition because the CDW wave vectors are never commensurate to the main phase, and indeed an additional structural transition occurs at lower temperature. In this regard, the intensity drop of the **q**1 satellites with decreasing temperatures observed in this work in $LaPt_2Si_2$ can be interpreted as follows: during the formation of the CDW at $T1$, the crystal lattice of $LaPt_2Si_2$ undergoes a structural distortion aimed at the accommodation of its lattice parameters and atomic positions to the CDW order. As a result, the positions of the Bragg reflections and their associated **q**1 satellites are shifted. With lowering temperature, the CDW transition at $T2$ occurs and interacts with the previously established CDW, as well as with the modified lattice structure. This transition introduces additional distortions in the lattice that are not compatible with the **q**1 modulation, hereby disrupting the periodicity of the initial CDW order, and causing a dramatic reduction in the intensity of the **q**1 satellite reflections. The intensity variations of the satellites are accompanied by as many structural transitions. Therefore, the **q**1 modulation of the cell is never compliant with neither the high nor the low-temperature *P*4/*nmm* crystal symmetry of $LaPt_2Si_2$. To interpret such a behavior the concept of discommensuration (DC) might be relevant in this case. DC was initially introduced theoretically by McMillan to explain the properties of 2H-$TaSe_2$[30]; here the incommensurate phase is regarded as a defect melting transition in which narrow domain walls separate large commensurate domains and, within such narrow domains, the superlattice phase fluctuates rapidly. Later on, this conjecture was confirmed with dark-field electron microscopy experiments[31], which provided direct observation of the commensurate and incommensurate domains and demonstrated that the CDW dislocation is the main responsible for the normal-to-incommensurate transition in 2H-$TaSe_2$. In the case under investigation, we have no direct evidence of DC. However, the metastable subtle structural changes in the main crystalline phase and the appearance of the higher-order satellites **q**2 related to **q**1, are experimental indications in support of the thesis that the CDW in $LaPt_2Si_2$ undergoes discommensuration, in qualitative agreement with the 2H-$TaSe_2$ case. Moreover, there are clear satellite intensity fluctuations in the full investigated temperature range (see Fig. 4), which can be interpreted as due to coherent interference from the ordered commensurate domains in the superlattice phase, in analogy to monolayer Kr/graphite thin film systems[32].

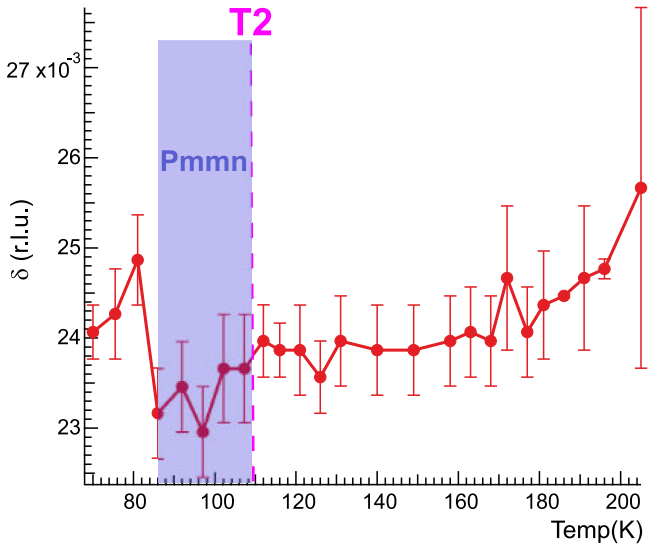

Fig. 7 Incommensurability of the q′1 satellites with respect to the main lattice in $LaPt_2Si_2$. The solid line is a guide to the eye, while the shaded purple area marks the temperature interval below T2 in which the degree of incommensurability, expressed in reciprocal lattice units, is minimum. The confidence intervals of the reported values are represented in the plots by the error bars on the experimental points.

Conclusions. The structural evolution and the temperature dependence of the development of the density wave state in the CDW superconductor $LaPt_2Si_2$ was clarified with synchrotron XRD and bulk characterization measurements. From our investigation, we concluded that the onset of the charge order is to be placed well above room temperature. On cooling, lattice distortions with multiple propagation vectors occur and their temperature evolution can be followed through the intensities of the corresponding Bragg satellites. In particular, four temperature regimes can be identified:

- $T > T1 = 230$ K: diffuse scattering is present in the *ab*-plane while broad scattering spots are already visible along the *c* axis. The crystal structure of $LaPt_2Si_2$ can be reliably refined with the tetragonal space group *P*4/*nmm*.
- $T2 < T < T1$: satellites with propagation vector $\mathbf{q}'1 = [0.36\ 0\ 0]$ and $\mathbf{q}''1 = [0\ 0.36\ 0]$ become sharp and their intensity increases on cooling. The crystal structure in $LaPt_2Si_2$ undergoes a second-order structural transition from the room temperature commensurate tetragonal phase to an incommensurate distorted tetragonal phase.
- $T3 < T < T2$: satellites with propagation vector $\mathbf{q}'2 = [0.18\ 0.18\ 0.5]$ and $\mathbf{q}''2 = [0.18\ -0.18\ 0.5]$ become sharp and their intensity increases on cooling. The crystal structure in $LaPt_2Si_2$ undergoes a first-order structural transition at $T = T2 = 110$ K from the incommensurate distorted tetragonal phase to a commensurate orthorhombic phase with space group *Pmmn*.
- $T < T3$: satellites with propagation vector $\mathbf{q}'3 = [0.3\ 0.3\ 0.25]$ and $\mathbf{q}''3 = [-0.3\ -0.3\ 0.25]$ appear and their intensity increases on cooling from $T3 = 60$ K. The tetragonal structure with space group *P*4/*nmm* is restored after a first-order transition.

A first CDW transition should be associated with the **q**1 satellites, the **q**2 satellites, associated to a second CDW transition, are related to the **q**1 as higher-order satellites, and the **q**3 modulation of the lattice is established as a consequence of the

structural instabilities induced by the charge modulation. First-order transitions towards commensurate crystal structures for the main cell occur in correspondence to the appearance of the **q**2 and **q**3 superstructures. The long 3D phase coherence length for the **q**1 and **q**2 propagation vectors implies strong inter-planar interactions among the Pt1 and Pt2 layers. This seems to indicate that two distinct CDW transitions occur: one at $T1$ with propagation vector **q**1 in the Pt2 layer, and one at $T2$ with propagation vector **q**2 in the Pt1 layer. The CDW-induced ion displacement indicates the presence of strong electron–phonon coupling, while the metastable structural changes, the appearance of higher-order satellites and their intensity fluctuations can be indications of discommensuration of the CDW in $LaPt_2Si_2$. This behavior is indeed similar to the behavior of other systems that manifest CDW discommensuration and dislocation. However, no direct evidence of DC is observed in this work, therefore, it is here presented as a speculative conjecture. The temperature-dependent behavior of the crystal structure and the evolution of the CDW-induced satellites clarified in this study seem to point toward an unconventional character of the $LaPt_2Si_2$ CDW states, with strong coupling between the Pt layers.

Methods

The synchrotron X-ray diffraction measurements were performed on the P21.1 beamline[33] at the PETRA III synchrotron facility of the DESY national research center (Deutsches Elektronen-Synchrotron). The sample was mounted on a Displex cold finger cryostat, with a T-range 10–320 K. The data were acquired with a PILATUS3 X CdTe 2M detector over 360° omega scans in 0. 1° steps. Data at 41 temperature points were collected on controlled heating in different steps depending on the range [10:10:50, 55:5:120, 130:10:150, 155:5:190, 200:10:300] K. The energy of the incoming photon beam was selected to be ≈102 keV. In the low-temperature region, there is a difference of about 10 K between the temperature readout in the proximity of the sample and the temperature set, therefore in this work we always refer to the sample temperature readout. The synchrotron XRD data were collected with three different attenuation settings: atten0 for zero attenuation, atten2 for intermediate attenuation, atten5 for maximum attenuation. Each attenuation step is achieved through 0.1 mm Tl. Due to the strong attenuation of the atten5 setting, not much information can be extracted from this dataset, therefore it was disregarded.

Preliminary in-house XRD data were collected at the Arrhenius Laboratory in Stockholm University. The resistivity and susceptibility measurements were performed at the Physical Properties of Materials laboratory at the Paul Scherrer Institute (PSI), Switzerland. The $LaPt_2Si_2$ sample was prepared using high-purity La, Pt, and Si at the Tata Institute of Fundamental Research (TIFR), Mumbai[34]. More specifically, the single crystal of $LaPt_2Si_2$ was grown by the Czochralski method. To begin with, a polycrystalline ingot of $LaPt_2Si_2$ weighing about 10 g was prepared using high-purity elements of La, Pt, and Si in the stoichiometric ratio of 1:1:2.1. From the ingot, a polycrystalline seed crystal was cut using a spark erosion cutting machine. A tetra-arc furnace was used to grow the single crystal. The polycrystalline ingot was melted again, and the seed crystal was gently inserted into the melt and pulled out rapidly at a rate of about 40 mm/h. After the necking process and stabilization of the growth conditions, the pulling was reduced to 10 mm/h. The grown crystal was subjected to Laue diffraction to ascertain the quality and to cut along the principal crystallographic directions. Well-defined Laue diffraction spots with fourfold symmetry confirmed the good quality of the single crystal (Fig. 8).

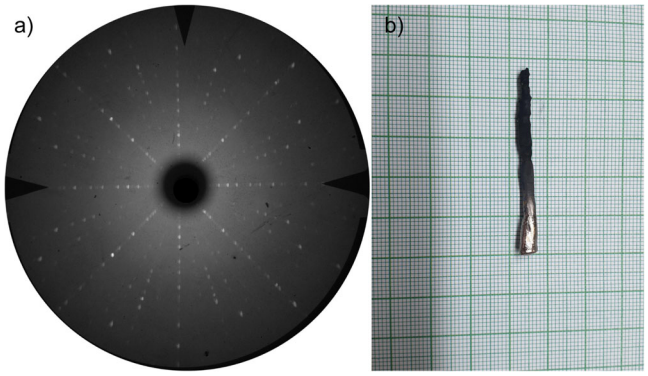

Fig. 8 Assessment of the $LaPt_2Si_2$ crystal quality. a Laue pattern for the (001)-plane of single-crystalline $LaPt_2Si_2$. **b** As-grown $LaPt_2Si_2$ single-crystal sample.

All images involving crystal structure were made with the VESTA software[35]. The XRD data reduction, unit cell determination, and refinement of the superstructural propagation vectors were carried out with the software CrysAlis^{Pro}[18]. The refinement of the underlying crystal structure in $LaPt_2Si_2$ was performed with the software SHELX[36]. The data plots were produced with the software IgorPro[37]. Crystallographic information files are provided as Supplementary Data 1–3 for the $LaPt_2Si_2$ 24 K structure, Supplementary Data 4–6 for the $LaPt_2Si_2$ 102 K structure, Supplementary Data 7–9 for the $LaPt_2Si_2$ 205 K structure, Supplementary Data 10–12 for the $LaPt_2Si_2$ 300 K structure.

Data availability

All the data of this work are available from the corresponding authors upon request. The data are also stored in the repositories of PETRA III and available from the P21.1 instrument responsible on request.

Received: 18 February 2023; Accepted: 15 September 2023;
Published online: 30 September 2023

References

1. da Silva Neto, E. H. et al. Ubiquitous interplay between charge ordering and high-temperature superconductivity in cuprates. *Science* **343**, 393–396 (2014).
2. Wagner, K. et al. Tuning the charge density wave and superconductivity in Cu_xTaS_2. *Phys. Rev. B* **78**, 104520 (2008).
3. Wang, A. et al. A crossover in the phase diagram of NaFe1-xCoxAs determined by electronic transport measurements. *New J. Phys.* **15**, 043048 (2013).
4. Chang, J. et al. Direct observation of competition between superconductivity and charge density wave order in $YBa_2Cu_3O_{6.67}$. *Nat. Phys.* **8**, 871–876 (2012).
5. Gupta, R., Paramanik, U., Ramakrishnan, S., Rajeev, K. & Hossain, Z. Coexistence of superconductivity and a charge density wave in $LaPt_2$(Si1-xGex)2 ($0 \leqslant x \leqslant 0.5$). *J. Phys. Condens. Matter* **28**, 195702 (2016).
6. Nagano, Y. et al. Charge density wave and superconductivity of RPt2Si2 (R= Y, La, Nd, and Lu). *J. Phys. Soc. Jpn.* **82**, 064715 (2013).
7. Hase, I. & Yanagisawa, T. Electronic structure of $LaPt_2Si_2$. *Phys. C Supercond.* **484**, 59–61 (2013).
8. Kim, S., Kim, K. & Min, B. The mechanism of charge density wave in pt-based layered superconductors: $SrPt_2As_2$ and $LaPt_2Si_2$. *Sci. Rep.* **5**, 1–10 (2015).
9. Aoyama, T. et al. 195Pt-NMR evidence for opening of partial charge-density-wave gap in layered $LaPt_2Si_2$ with CaBe2Ge2 structure. *J. Phys. Soc. Jpn.* **87**, 124713 (2018).
10. Kubo, T. et al. Structural phase transition and superconductivity in $LaPt_2Si_2$: 139La-and 195Pt-NMR studies. in *Proceedings of the International Conference on Strongly Correlated Electron Systems (SCES2013)*, JPS Conference Proceedings, 017031 (2014).
11. Falkowski, M., Doležal, P., Andreev, A., Duverger-Nédellec, E. & Havela, L. Structural, thermodynamic, thermal, and electron transport properties of single-crystalline $LaPt_2Si_2$. *Phys. Rev. B* **100**, 064103 (2019).

12. Falkowski, M. et al. Multiple charge density wave states and magnetism in $NdPt_2Si_2$ against the background of its nonmagnetic analog $LaPt_2Si_2$. *Phys. Rev. B* **101**, 174110 (2020).
13. Das, D. et al. Multigap superconductivity in the charge density wave superconductor $LaPt_2Si_2$. *Phys. Rev. B* **97**, 184509 (2018).
14. Nie, Z. et al. Nodeless superconductivity in the charge density wave superconductor $LaPt_2Si_2$. *Phys. Rev. B* **103**, 014515 (2021).
15. Kittel, C. & McEuen, P. *Introduction to Solid State Physics* (John Wiley & Sons, 2018).
16. Zhu, X., Guo, J., Zhang, J. & Plummer, E. Misconceptions associated with the origin of charge density waves. *Adva. Phys. X* **2**, 622–640 (2017).
17. Naito, M. & Tanaka, S. Electrical transport properties in 2H-NbS_2,-$NbSe_2$,-TaS_2 and-$TaSe_2$. *J. Phys. Soc. Japn.* **51**, 219–227 (1982).
18. CrysAlis PRO: Agilent. CrysAlis PRO. Agilent Technologies Ltd, Yarnton, Oxfordshire, England (2014).
19. Augieri, A. et al. Correlated disorder in YBCO and composite YBCO films revealed by means of synchrotron x-ray diffraction. *IEEE Trans. Appl. Supercond.* **28**, 1–4 (2018).
20. Nocerino, E. et al. Q-dependent electron-phonon coupling induced phonon softening and non-conventional critical behavior in the CDW superconductor $LaPt_2Si_2$. *J. Sci. Adv. Mater. Devices* **8**, 100621 (2023).
21. Lingannan, G. et al. Pressure-dependent modifications in the $LaAuSb_2$ charge density wave system. *Phys. Rev. B* **103**, 195126 (2021).
22. Petříček, V., Dušek, M. & Palatinus, L. Crystallographic computing system jana2006: general features. *Zeitschrift für Kristallographie-Crystalline Mater.* **229**, 345–352 (2014).
23. Ivantchev, S., Kroumova, E., Madariaga, G., Perez-Mato, J. & Aroyo, M. SUBGROUPGRAPH: a computer program for analysis of group–subgroup relations between space groups. *J. Appl. Crystallogr.* **33**, 1190–1191 (2000).
24. Authier, A. *International Tables for Crystallography: Volume D: Physical Properties of Crystals* (Wiley Online Library, 2003).
25. Hwang, C., Meichle, M., Salamon, M. & Wayman, C. Transformation behaviour of a $Ti_{50}Ni_{47}Fe_3$ alloy I. premartensitic phenomena and the incommensurate phase. *Philos. Mag. A* **47**, 9–30 (1983).
26. Kawasaki, S. et al. Coexistence of multiple charge-density waves and superconductivity in $SrPt_2As_2$ revealed by As75- NMR/NQR and Pt195-NMR. *Phys. Rev. B* **91**, 060510 (2015).
27. Moncton, D., Axe, J. & DiSalvo, F. Study of superlattice formation in 2H-$NbSe_2$ and 2H-$TaSe_2$ by neutron scattering. *Phys. Rev. Lett.* **34**, 734 (1975).
28. Wilson, J. A., Di Salvo, F. & Mahajan, S. Charge-density waves and superlattices in the metallic layered transition metal dichalcogenides. *Adv. Phys.* **24**, 117–201 (1975).
29. McMillan, W. Landau theory of charge-density waves in transition-metal dichalcogenides. *Phys. Rev. B* **12**, 1187 (1975).
30. McMillan, W. L. Theory of discommensurations and the commensurate-incommensurate charge-density-wave phase transition. *Phys. Rev. B* **14**, 1496 (1976).
31. Chen, C., Gibson, J. & Fleming, R. Direct observation of charge-density-wave discommensurations and dislocations in 2H-TaSe2. *Phys. Rev. Lett.* **47**, 723 (1981).
32. Stephens, P., Heiney, P., Birgeneau, R. & Horn, P. X-ray scattering study of the commensurate-incommensurate transition of monolayer krypton on graphite. *Phys. Rev. Lett.* **43**, 47 (1979).
33. Dippel, A.-C., Zimmermann, M. V., Staron, P. & Schneider, J. R. Examples of high-energy X-ray structural studies at PETRA III: High TC superconductors, real-time surface and thin film processes, and design of engineering materials. *Synchrotron Radiat. News* **33**, 24–30 (2020).
34. Gupta, R., Dhar, S., Thamizhavel, A., Rajeev, K. & Hossain, Z. Superconducting and charge density wave transition in single crystalline LaPt2Si2. *J. Phys. Condens. Matter* **29**, 255601 (2017).
35. Momma, K. & Izumi, F. VESTA: a three-dimensional visualization system for electronic and structural analysis. *J. Appl. Crystallogr.* **41**, 653–658 (2008).
36. Sheldrick, G. M. Crystal structure refinement with SHELXL. *Acta Crystallogr. Sec. C Struct. Chem.* **71**, 3–8 (2015).
37. WaveMetrics. IGOR Pro, scientific data analysis software (2016). http://www.wavemetrics.com/products/igorpro/igorpro.htm.

Acknowledgements

We acknowledge DESY (Hamburg, Germany), a member of the Helmholtz Association HGF, for the provision of experimental facilities. Parts of this research were carried out at PETRA III, and we would like to sincerely thank O. Ivashko, M. von Zimmermann and P. Glaevecke for assistance in using P21.1. Beamtime was allocated for proposal 11013546. The bulk measurements were carried out at the Laboratory for Multiscale Materials Experiments, Paul Scherrer Institut, in Switzerland. The authors wish to thank the staff of PSI for the valuable support provided during the measurements. The initial in-house XRD characterization was carried out at the Stockholm University, Arrhenius Laboratory (Department of Materials and Environmental Chemistry). The authors wish to thank A.K. Inge for the valuable support provided during the measurements, as well as A. Geresdi and N. Trnjanin, from the Chalmers University of Technology, for the enlightening discussions around unconventional superconductors. This research is funded by the Swedish Foundation for Strategic Research (SSF) within the Swedish national graduate school in neutron scattering (SwedNess). Y.S. acknowledges funding from the Swedish Research Council (VR) through a Starting Grant (Dnr. 2017-05078) and Area of Advances-Material Sciences from Chalmers University of Technology. Y.S. is also supported by Wallenberg Young Fellow through the grant KAW 2021.0150. A.M. would like to acknowledge financial support from the E.R.C. (Grant 788144).

Author contributions

E.N. conceived the experiments. E.N., M.Me., J.L., Y.M.K., O.I., M.v.Z., and K.P. conducted the experiments. E.N., I.S., A.M., K.L., Y.S., and M.Må. analyzed the results. The samples were synthesized by Z.H. and A.T. who also conducted the initial sample characterizations. E.N. and M.Må. made all the figures. E.N. created the first draft, and all co-authors reviewed and revised the manuscript.

Funding

Open access funding provided by Royal Institute of Technology.

Competing interests

The authors declare no competing interests.

Additional information

Supplementary information The online version contains supplementary material available at https://doi.org/10.1038/s43246-023-00406-y.

Correspondence and requests for materials should be addressed to Elisabetta Nocerino or Martin Månsson.

Peer review information *Communications Materials* thanks Gaetano Campi and the other, anonymous, reviewer(s) for their contribution to the peer review of this work. Primary Handling Editors: Nicola Poccia and Aldo Isidori.